Supplemental Information

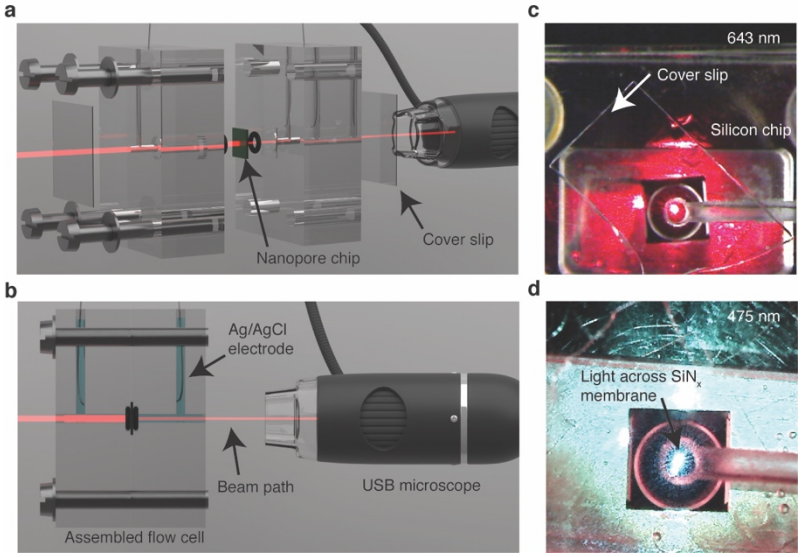

Figure S1: **Experimental Set-Up. a,** Two parts of a poly(methyl methacrylate) (PMMA) flow-cell are screwed together to sandwich the nanopore chip (indicated by an arrow) between two O-rings. After filling the flow-cell with electrolyte, the two inlets are sealed with a cover slip (indicated by an arrow). A USB microscope is used to monitor the laser beam. **b,** Sideview of the experimental set-up. The Ag/AgCl electrodes are placed outside of the laser beam path. **c,** Example alignment using the 643nm laser. The laser light only passes across nanopore chip when the beam is properly aligned to the SiN_x membrane. The ideal position of the nanopore chip is found by maximizing the transmitted light. **d,** An example alignment using the 475 nm laser.

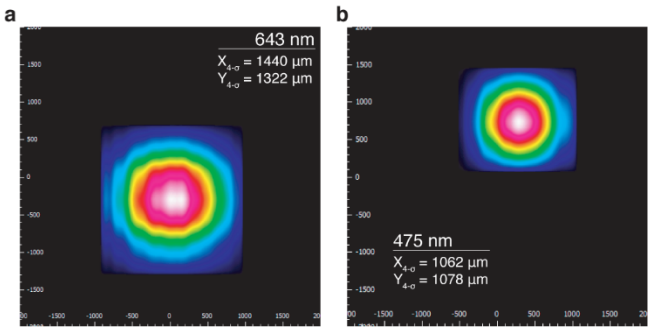

Figure S2: **Laser Characteristics.** Measured laser spot sizes for laser the two diode lasers with wavelengths 643 nm (**a**) and 475 nm (**b**).

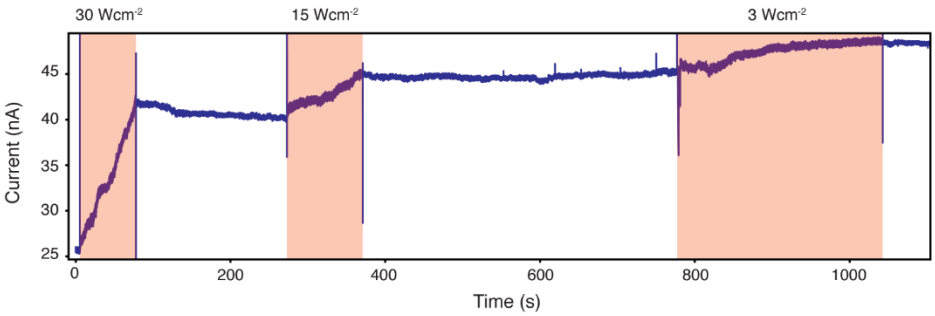

Figure S3: **Nanopore Enlargement.** Enlargement of the nanopore for different photon fluxes for the 643nm laser

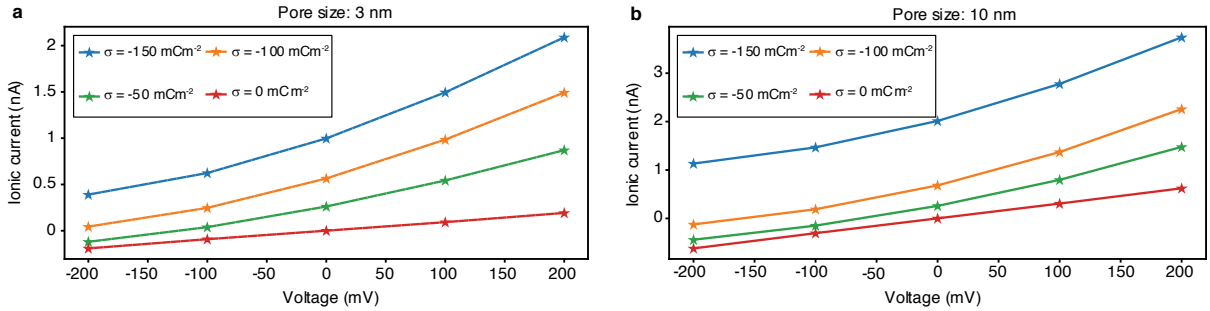

Figure S4: **Simulated effect of the surface charge.** Simulated I-V characteristics for the 3 nm (**a**) and 10 nm (**b**) pore. The experimentally observed upwards shift of the I-Vs is reproduced by this COMSOL model.

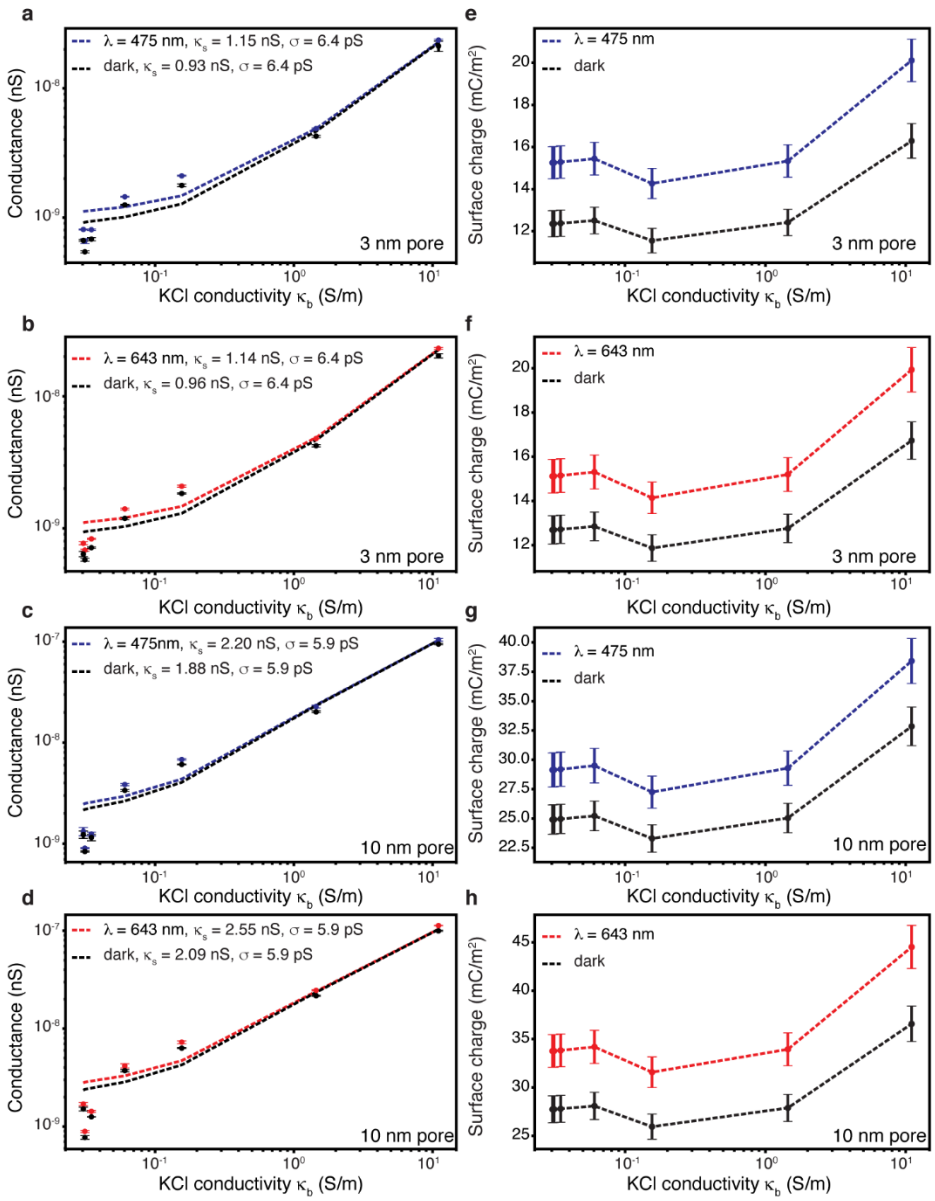

Figure S5: **Surface charge measurements a-d,** Conductance measurements (triplicates) of a 3 nm (**a-b**) and a 10 nm (**c-d**) pore for different KCl conductivities and different laser wavelengths (**a,c**: 475 nm, **b,d**: 645 nm). The dashed lines denote the fit of the conductance equation (Equation (1)) to extract the surface conductance κ_b. These values are then used to calculate the surface charge at each measurement point (**e-h**). The error bars in **a-d** are the spread of the datapoints of the triplicate measurement. In **e-h** the error bars are estimated through error propagation. A detailed analysis and information on the error propagation can be found in the Supplemental Information. The flux of the 643 nm and the 475 nm laser were 0.75 Wcm^{-2} and 1.3 Wcm^{-2}, respectively.

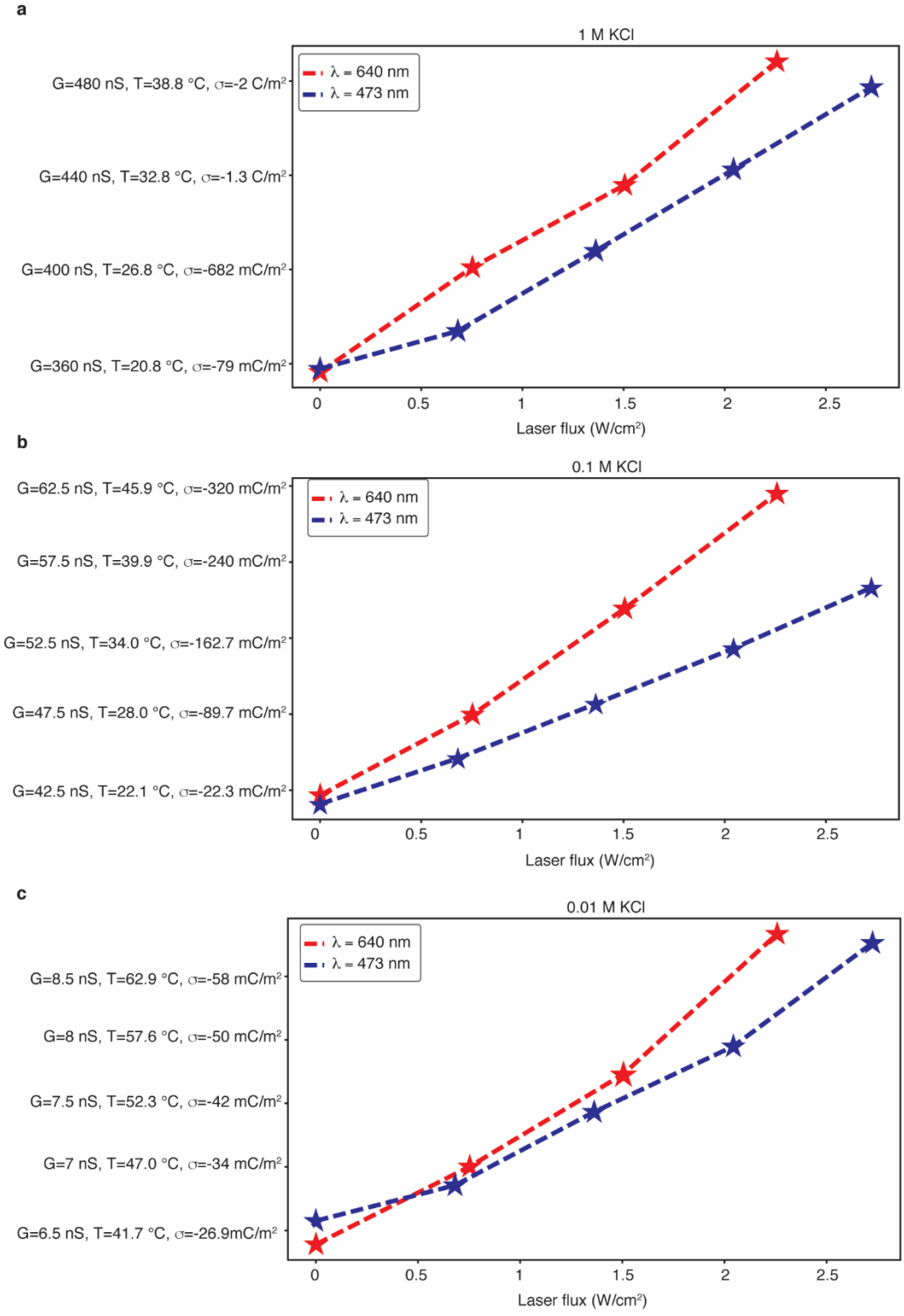

Figure S6: **Heat calculation.** Laser influence on the conductance of a silicon nitride nanopore at concentrations of 1 M (**a**), 100 mM (**b**) and 10 mM (**c**) KCl. The conductance G is measured, whereas the temperature T and the surface charge σ are calculated according to the main text in order to estimate the necessary temperature or surface charge change to explain the observed data.

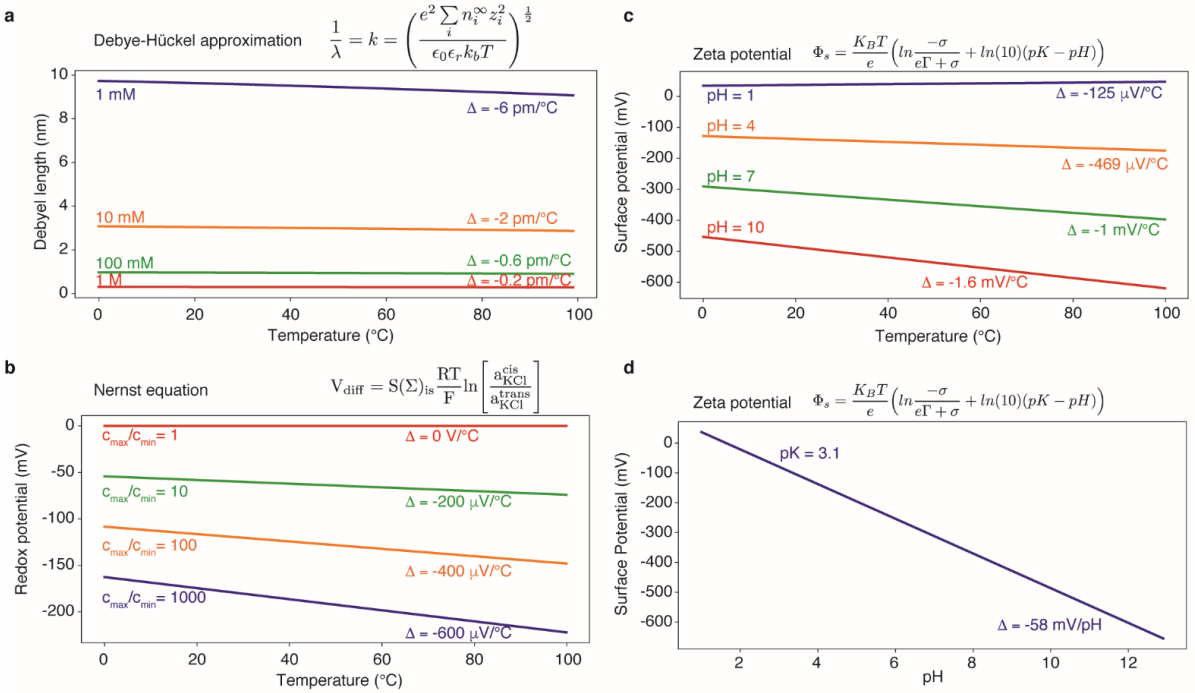

Figure S7: **Analytical heat estimation. a,** Debye Length vs temperature for different ionic dilutions. The data has been calculated using the Debye-Hückel approximation[38] and an analytical estimation of the dielectric constant of water[39]. **b,** Nernst potential vs. temperature for different concentration gradients. **c,** The surface potential vs temperature for different pH values. **d,** The surface potential as a function of pH for assuming a pK of 3.1.

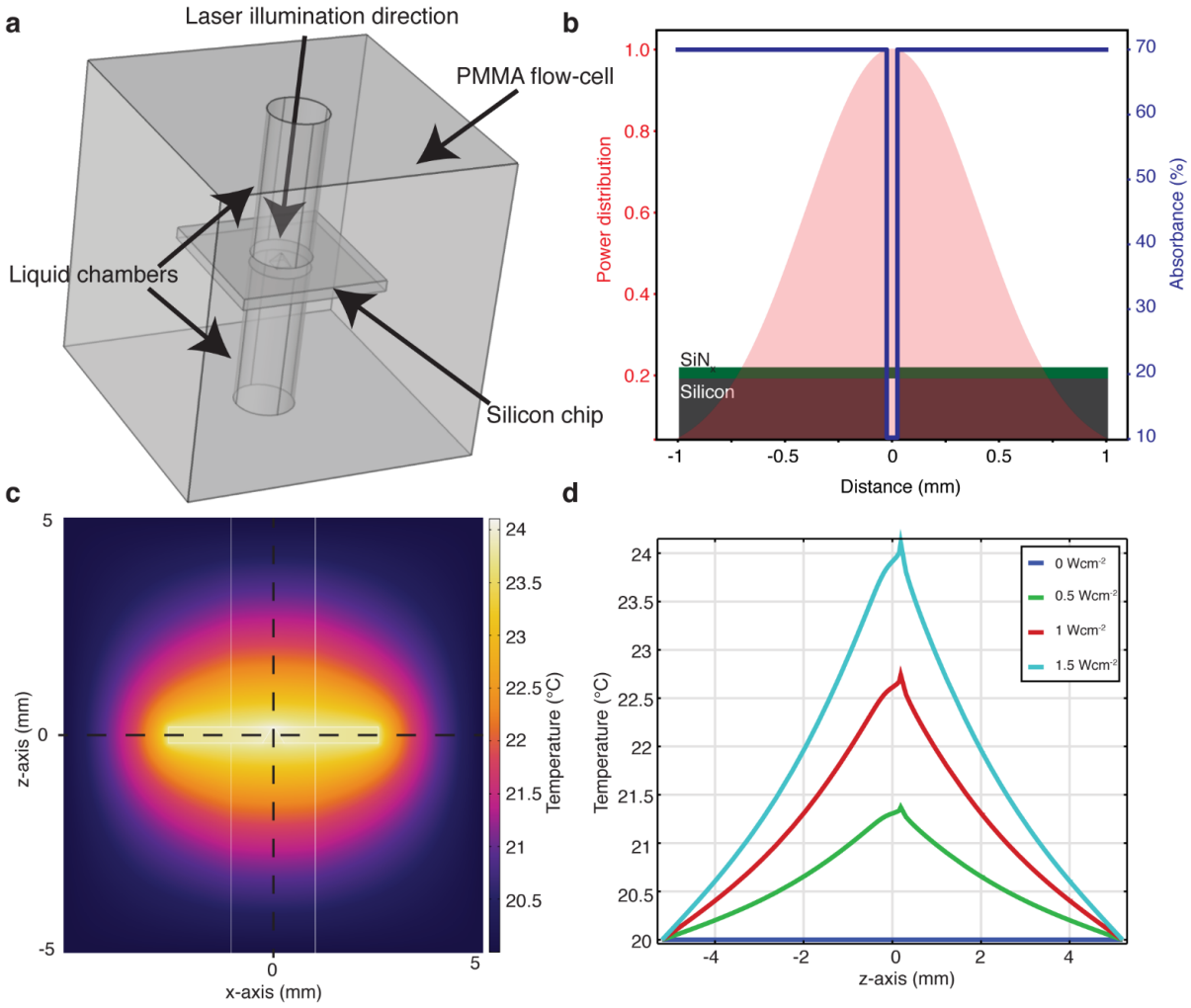

Figure S8: **FEM simulation of the heat generated by the laser light. a,** The geometry of the model used to reproduce as closely as possible the experimental situation. **b,** Illustration of the power distribution irradiating the surface of the chip (red) and the different absorbance values over the surface. **c,** Heat map of the z-x axis of the system. **d,** The temperature profile along the z-axis and through the centre of the membrane

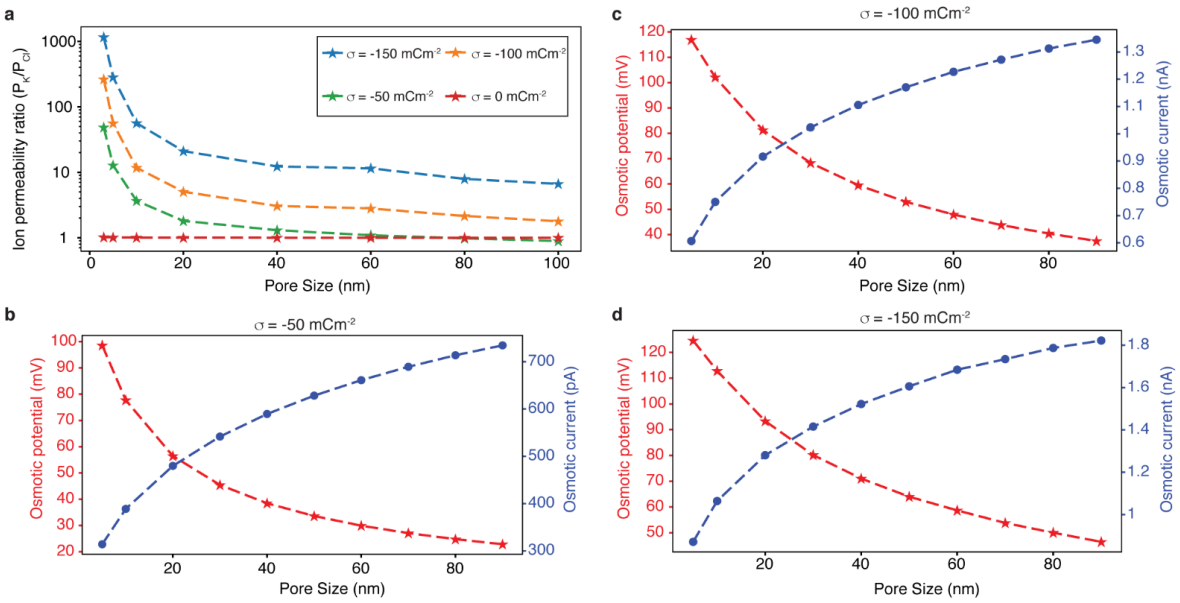

Figure S9: **Permeability ratio simulations. a,** Simulated permeability ratio. **b-d,** Osmotic potential and current versus pore sizes for surface charges of -50 mC m^{-2} (**b**), -100 mC m^{-2} (**c**) and -150 mC m^{-2} (**d**).

Set power [mW]	Real power 643 nm [mW]	Real power 475 nm [mW]
150	135.9	-
140	127.1	-
130	117.9	-
120	109.1	-
100	91.7	98.3
50	47.1	49.1
20	19.89	19.6
10	10.7	9.76
1	1.8	-

Table S1: **Laser powers.** The *set power* is the power value entered in the program. The *real power* is the corresponding power measured with a power meter.

Salt Concentration	Measured Potential	Potential Difference (with respect to 1M)	Theoretical
1 M	31.7 mV	0 mV	0 mV
10 mM	82.9 mV	51.2 mV	58.6 mV
100 mM	135 mV	103.3 mV	117.13 mV
1 mM	185 mV	153.3 mV	175.7 mV

Table S2: **Measurement of the redox potential at the Ag/AgCl electrodes**

10 nm pore	643 nm		475nm	
	Dark	752 µW/cm²	Dark	1.3 mW/cm²
Osmotic current	1.41 nA	1.63 nA	1.32 nA	1.48 nA
Osmotic voltage	95.64 mV	98.63 mV	92.30 mV	95.37 mV
Osmotic power	134.72 pW	160.85 pW	122.09 pW	140.66 pW

3 nm pore	643 nm		475nm	
	Dark	752 µW/cm²	Dark	1.3 mW/cm²
Osmotic current	172.76 pA	291.34 pA	207.99 pA	283.98 pA
Osmotic voltage	71.03 mV	98.20 mV	73.21 mV	91.86 mV
Osmotic power	12.41 pW	28.67 pW	15.33 pW	26.27 pW

Table S3: **Overview of results.** Mean values of the dataset reported in Figure 2

Supplemental Experimental Procedures

Calculation of the heat influencing the system

First, we set out to estimate the heating effect of the laser power when it penetrates through water. We used the following equation derived by Peterman et al.[40] to estimate the steady state change of temperature ΔT: $\Delta T = \frac{\alpha}{2\pi \cdot C} \cdot [ln(\frac{2\pi \cdot R}{\lambda}) - 1] \cdot P$, where α is the absorption coefficient (*0.0114 for 475 nm and 0.322 for 643 nm*[41]), λ the wavelength of the laser used, P the laser power (150 mW, full theoretically possible power), C the thermal conductivity of water (0.60 $Wm^{-1}K^{-1}$) and R the distance to the surface of the flow cell. For both wavelengths, the temperature increases are below 0.01 °C, which means that we can neglect any heating effects of the water.

Since we are working with a non-focused laser of about 1 mm spot size (Figure S2) we irradiate not only the silicon nitride membrane but also some of the silicon that is found outside the membrane. To estimate the heat produced by this system we simulated the geometry in COMSOL. We designed a 50 µm squared, 20 nm thick nitride membrane in a 5 mm dice of silicon. Water is placed in a circular fashion on top and on the bottom of the chip. A 10x10mm PMMA block is placed around the system and the outer boundaries of this block have been set to room temperature. An illustration of the simulated geometry can be found in Figure S8a. The silicon nitride window and the silicon are treated separately using two instances of the *deposited beam power* module. Since the silicon nitride window is transparent, we assume an absorbance value of only 10% as previously calculated[42]. On the other hand, the absorbance of the silicon part was set to 70%, since 30% of the light gets reflected on its polished surface[43] (Figure S8b). The spot size to calculate the power flux was set to 1mm, whereas the deposited Gaussian beam profile was set to a standard deviation of 250 µm to correspond to the commonly used 4-σ value of beam width. The resulting temperature profile in the case of a 1.5 $mWcm^{-2}$ intensity can be found in Figure S8c. Figure S8d shows the temperature distribution along the z-axis of the nanopore chip for different laser powers. A small peak is found at the nitride membrane. In general, the highest possible temperature increase at its peak value is about 4 °C. These values are absolute upper limits, since we do not take into account any losses happening due to scattering on the PMMA flow cell and intensity losses when the light penetrates the glass slide covering the flow cell. We can expect the real temperature increases to be substantially lower than the values estimated here.

In this part we estimate and rule out the influence of temperature on the observed results. Here, we ignore any influence of the surface charge and concentrate on the temperature dependence of the KCl conductivity. Electrolytic conductivity (σ) values of KCl (concentrations ranging from 10 mM to 1

M) in a temperature (T) range of 0 to 50 °C were extracted from the NIST standards for electrolytic conductivity[44]. Since the conductivity-temperature relationship is linear in this range, we extracted parameters *a* and *b* from: $\sigma = a \cdot T + b$. We can then extract the temperature corresponding to a certain nanopore conductance using: $T = \frac{\sigma - b}{a}$, where $\sigma = G \cdot [\frac{4l}{\pi D^2} + \frac{1}{D}]^{-1}$ [20], where *G* is the conductance, *D* the pore diameter, *l* the pore length and σ the ionic conductivity. In these calculations, we assume that the pore diameter and length does not change. We used a suspended MoS_2 layer in a 70 nm nitride hole. In this configuration, the MoS_2 layer reaches until the nitride edge producing a pore of diameter 70 nm and a thickness of 21 nm (20 nm nitride + ~1 nm MoS_2). The advantage of this configuration is its higher temporal stability. In Figure S6 we measured the conductance of this nanopore at different symmetric salt concentrations of 1 M, 100 mM and 10 mM. If we apply the same temperature analysis, we observe that higher temperature differences are needed to explain the data at low salt concentration (up to 60 °C). This is not consistent with the reasonable assumption that the laser heating is independent of the ion concentration. There must be another, concentration dependent variable at play: the surface charge.

Other than viscosity changes, heat also influences the chemical potential difference. We can express the osmotic voltage observed in Figure 2 in a simplified way using the reversal potential: $V_{diff} = S(\Sigma)_{is} \frac{RT}{F} \cdot ln[\frac{c_{cis}}{c_{trans}}]$, where V_{diff} is the measured osmotic potential, $S(\Sigma)_{is}$ the ion selectivity, and the logarithmic expression the concentration gradient. To estimate the pure thermal effect, we assume that the laser is not influencing the ion selectivity, so we set $S(\Sigma)_{is}$ to a fixed value (selectivity in the dark state) and vary T in order to obtain the values measured. In the case of the smaller, 3 nm pore, a temperature differences of 118 °C and 73.9 °C are needed to explain the change due to a 643 nm and 475 nm laser irradiation. For exactly the same laser conditions these values drop to 11.5 °C and 6.5 °C for the 10 nm pore. Realistically, no difference should be seen between the two cases since an enlarged nanopore does not influence how the laser heats the system. Furthermore, the values obtained for the small nanopore are at least an order of magnitude away from anything we could expect from the previous estimation.

In order to estimate the influence of the temperature on the EDL we analytically calculate the thickness of the EDL for different temperature (Figure S7). The thickness of the EDL corresponds to the Debye length. With the Debye-Hückel approximation we can calculate the Debye length λ as[38]: $\frac{1}{\lambda} = \kappa = (\frac{e^2 \sum n_i^\infty z_i^2}{\varepsilon_0 \varepsilon_r k_B T})^{\frac{1}{2}}$, where κ is the Debye-Hückel parameter, ε_r the relative permittivity of water, ε_0 the permittivity of vacuum, k_B Boltzmann's constant, *T* temperature, n_i the bulk volume density, z_i the valence (in the case of KCl: $\sum n_i^\infty z_i^2 = 2n^\infty$) and *e* the electron charge. Since ε_r depends on the temperature as well we can use an analytical approximation to calculate its value[39]. Since the EDL length actually decreases a few picometers per °C of increased temperature, we cannot expect to see any improvement of the pore ion selectivity due to temperature changes and EDL thickness.

The surface charge of MoS_2 in water is estimated through the following chemical equilibrium:

$$MoS_2 + H_2O \rightleftharpoons MoS_2 - OH^- + H^+$$

We can estimate the diffuse layer electrostatic potential Φ_s (Zeta potential) of the surface by[45,46]: $\Phi_s = \frac{K_B T}{e}(ln\frac{-\sigma}{e\Gamma + \sigma} + ln(10)(pK - pH))$, where σ is the surface charge and Γ the density of reactive sites. The pK of nanocrystalline MoS_2 has been measured to be around 3.1[47]. We estimate the surface potential at different temperatures and pH using a pK value of 3.1 and a surface charge value of -50 mC m^{-2}. The surface potential changes with temperature, but the rate of this change is highly dependent on the pH as calculated in Figure S7c. For instance, at pH 7 the rate is just below 1 mVK^{-1} whereas at pH 4 the rate is only about 640 μVK^{-1}. Such an increase in surface potential might well

improve the repulsion of cations and therefore increase the ion selectivity. Assuming we get a temperature increase of 10 °C then we could expect a 10 mV stronger surface potential. To put this value into context we can estimate the pH change needed to induce the same increase in surface potential. From Figure S7d we can see that the surface potential reduces 58 mV per pH unit. In order to get a 10 mV decrease, we would thus need a pH change of roughly 0.2, which is well within the error of our buffer system, especially at low dilutions.

Last but not least, the redox potential generated at the interface of the Ag/AgCl electrode with the ionic solution also depends on the temperature. Depending on the salt concentration the potential can increase between 200 and 600 μVK^{-1} (Figure 7b). This is relevant if the whole system is heated and has to be considered if one wants to calculate the effective osmotic power generated by the membrane. In the case of laser irradiation, we can neglect any influences originating from the redox potential since we are not affecting the temperature that far away from the membrane.

Derivation of the modified GHK equation

Deviations in conductance from bulk predictions have been observed in nanopores with high aspect ratios L/D<1[13] and were linked to a large contribution of the surface conductivity, described as the ratio between surface and bulk conductivity: $l_{Du} = \frac{\kappa_s}{\kappa_b}$, where κ_s is the surface conductivity and κ_b the bulk conductivity. This Dukhin length, l_{Du}, can be approximated using the surface charge σ and the bulk ion concentration c_s as: $l_{Du} \approx \frac{\sigma}{2 \cdot c_s \cdot e}$. The surface charge of the MoS^2 membrane was fixed to -50 mCm^{-2} as previously determined[4]. The Dukhin lengths on both sides are then 2.6 and 26 nm respectively (Figure 4a). Since this formalism has been developed for symmetrical salt concentrations, we set the effective Dukhin length to 2.6 nm and thus provide the lower limit of the effect by underestimating the surface conduction effect. To further quantify the contributions of the surface and bulk conductance to the ionic current inside the pore, we refer to the Dukhin number which is defined as: $Du = \frac{4 \cdot l_{Du}}{D}$, where *D* is the pore diameter[13]. The Dukhin number of the 3 nm pore is 3.5 suggesting a large surface conductance contribution, whereas the 10 nm has Du = 1 (equal contributions). In order to calculate the osmotic voltage in the surface conductance dominated regime, we need to know the distribution of the ions in the vicinity of the membrane. Using FEM simulations, we estimate these ion concentrations as a function of distance to a charged membrane (σ= -50 mC m^{-2}, Figure 4b). We then take the mean concentration from the wall (x = 0) to a distance x = λ (where λ is the Debye length, λ = 1 nm for cis side and λ = 9.6 nm on the trans side) to estimate the concentrations at the membrane surface: $c_{K^+}^{trans}$, $c_{Cl^-}^{trans}$, $c_{Cl^-}^{cis}$ and $c_{K^+}^{cis}$. The bulk concentrations of potassium and chloride are identical and simply denoted as c_{cis} and c_{trans}. We rewrite the GHK equation to account for the surface conductance as well as the bulk conductance:

$$E_{total} = \frac{RT}{F}[R_b \cdot ln(\frac{P_{K^+/Cl^-} \cdot c_{cis} + c_{trans}}{P_{K^+/Cl^-} \cdot c_{trans} + c_{cis}}) + R_s \cdot ln(\frac{P_{K^+/Cl^-} \cdot c_{K^+}^{cis} + c_{Cl^-}^{trans}}{P_{K^+/Cl^-} \cdot c_{K^+}^{trans} + c_{Cl^-}^{cis}})]$$

Where P_{K^+/Cl^-} is the permeability ratio, R_b and R_s are the contribution ratios of the bulk conductance and surface conductance that satisfy $R_s + R_b = 1$ and are estimated using the Dukhin number: $R_b = \frac{1}{1+Du}$ and $R_s = \frac{Du}{1+Du}$, effectively scaling the reverse potential to surface and bulk contributions. We estimate the permeability values P_{K^+/Cl^-} by geometrically estimating the area affected by the EDL inside the pore:

$P_{K^+/Cl^-}(D) = P_{max} \frac{A_{EDL}}{A_{total}} = P_{max} \frac{\pi(\frac{D}{2})^2 - \pi(\frac{D}{2} - \lambda)^2}{\pi(\frac{D}{2})^2}$, which can be simplified to $P_{K^+/Cl^-}(D) = 4\lambda \cdot P_{max} \frac{D-\lambda}{D^2}$. The Debye length, λ, was defined as 1 nm inside the nanopore. The value of the maximal permeability ratio, P_{max} was chosen to be 100 to best reflect the values obtained through FEM simulations (Figure S9a) and experimental studies[5].

Surface Charge Measurements

In order to estimate the influence of the laser light on the MoS_2 surface charge, we performed conductance measurements in KCl electrolyte with different conductivities. The analysis of the surface charge is based on the work of Lee et al.[13], who developed an analytical expression of the nanopore conductance *G* by taking into account the surface conductance:

$$G = \kappa_b[\frac{4l}{\pi D^2} + \frac{1}{1+4\frac{l_{Du}}{d}} + \frac{2}{\alpha d + \beta l_{Du}}]^{-1} \quad (1)$$

, where κ_b is the bulk conductivity, *l* the pore thickness, *D* the pore diameter and the geometrical factors $\alpha = \beta = 2$. As previously mentioned l_{Du} is the Dukhin length defined as $l_{Du} = \frac{\kappa_s}{\kappa_b}$. We prepared dilutions of KCl electrolyte with the following measured conductivities κ_b (in S m^{-1}): 0.0303, 0.0311, 0.0347, 0.0605, 0.3123, 1.447 and 11.03. We then measured the ionic conductance of our nanopore system for a 3 nm and a 10 nm pore with and without laser illumination (λ = 643 nm and λ = 475 nm). The conductance is estimated from the slope of the linear I-V characteristics. All measurements were taken in triplicates. In Figure S5a-d we show the obtained conductance values for each conductivity (circles). The error bars range from minimal to maximal measured value, emphasizing the reproducibility of the measurement. We use this measured relationship between nanopore conductance and KCl conductivity to estimate the surface conductance κ_s of equation (1). This is done through a curve fit. The fit (dashed line) and the obtained values for the surface conductance are reported in Figure S5a-d. We can calculate the surface charge σ for a given κ_s through the relationship:

$$\sigma \approx 2 \cdot c \cdot e\frac{\kappa_s}{\kappa_b} \quad (2)$$

where *c* is the ion concentration and *e* the elementary charge. We know that preparing very low dilutions of KCl can be very challenging in practice, we estimate the effective ion concentration for a given buffer from the measured conductivity κ_b. We use the Kohlrausch's law to convert the conductivities to ion concentration[48]:

$$\Lambda = \Lambda^0 - (A + B\Lambda^0)\sqrt{c} \quad (3)$$

, where Λ is the molar conductivity ($\frac{\kappa_b}{c}$), *A* = 60.20 and *B* = 0.229 constants and Λ^0 = *149.79 m^2 S mol^{-1}* the molar conductivity at infinite dilution. Figure S5c-h shows the resulting surface charges for the different conditions. The apparent increase of the surface charge for the high κ_b value is due to a simplification in Equation (2), which leads to overestimation of the surface charge in highly concentrated KCl solutions[13].

The error bars S_σ are estimated through propagating the errors using the variance formula:

$$S_\sigma = \sqrt{(\frac{2e\kappa_s}{\kappa_b})^2 \cdot S_c^2 (\frac{2ce}{\kappa_b})^2 \cdot S_{\kappa_s}^2 + (\frac{2ce\kappa_s}{\kappa_b^2})^2 \cdot S_{\kappa_b}} \quad (4)$$

, where S_{κ_b} is the error in the conductivity measurement (estimated to be 5%), S_{κ_s} the uncertainty of the fit and S_c the error in estimating the ion concentration (estimated to be 10%).

Supplemental References

38. Schoch R.B., Han J., Renaud P. (2008). Transport phenomena in nanofluidics. Rev. Mod. Phys. 80, 839–883.
39. Malmberg C.G., Maryott A.A. (1956). Dielectric constant of water from 0 to 100 C. J. Res. Natl. Bur. Stand. (1934). 56, 1.
40. Peterman E.J.G., Gittes F., Schmidt C.F. (2003). Laser-induced heating in optical traps. Biophys. J. 84, 1308–1316.
41. Pope R.M., Fry E.S. (1997). Absorption spectrum (380–700 nm) of pure water II Integrating cavity measurements. Appl. Opt. 36, 8710.

42. Yamazaki H., Hu R., Henley R.Y., Halman J., Afonin K.A., Yu D., Zhao Q., Wanunu M. (2017). Label-Free Single-Molecule Thermoscopy Using a Laser-Heated Nanopore. Nano Lett. 17, 7067–7074.
43. Green M.A. (2008). Self-consistent optical parameters of intrinsic silicon at 300 K including temperature coefficients. Sol. Energy Mater. Sol. Cells 92, 1305–1310.
44. Cline J.P. (2004). Accuracy in powder diffraction III - Part 1 - Preface. J. Res. Natl. Inst. Stand. Technol. 109, iii.
45. Van Der Heyden F.H.J., Stein D., Dekker C. (2005). Streaming currents in a single nanofluidic channel. Phys. Rev. Lett. 95, 116104.
46. Huang Z., Zhang Y., Hayashida T., Ji Z., He Y., Tsutsui M., Miao X.S., Taniguchi M. (2017). The impact of membrane surface charges on the ion transport in MoS_2 nanopore power generators. Appl. Phys. Lett. 111, 263104.
47. Ge P., Scanlon M.D., Peljo P., Bian X., Vubrel H., O'Neill A., Coleman J.N., Cantoni M., Hu X., Kontturi K., et al. (2012). Hydrogen evolution across nano-Schottky junctions at carbon supported MoS_2 catalysts in biphasic liquid systems. Chem. Commun. 48, 6484.
48. Vanysek P.V. Equivalent Conductivity of Electrolytes In Aqueous Solution. URL: https://sites.chem.colostate.edu/diverdi/all_courses/CRCreferencedata/equivalentconductivityofelectrolytes.pdf (visited on 02/05/2019).